Proceedings of the ASME 2019
International Mechanical Engineering Congress and Exposition
IMECE2019
November 11-14, 2019, Salt Lake City, UT, USA

IMECE2019-10171

ESTIMATED FLUID FORCE AND DAMPING CHARACTERISTICS OF A THIN FILM DAMPER COMPARISON BETWEEN CLOSED-FORM SOLUTIONS AND NUMERICAL ANALYSIS (DRAFT)

Jason T. Cook
Oak Ridge National Laboratory*
Oak Ridge, TN, USA

ABSTRACT

Analytical solutions of thin film dampers are useful for determining critical speeds and stability of rotor systems. Most thin film dampers in use are of short axial length, and closed-form solutions to the Reynolds equations exist for estimating pressure, forces, and damping for these types of dampers. This article compares the fluid film forces and damping estimated by the short film bearing model form of the Reynolds equations to the calculated forces and damping of a transient computational fluid dynamic simulation. For this comparison, the fluid was assumed to be incompressible, laminar, and isoviscous. The fluid film forces and damping are calculated from integrating the pressure distribution over the surface of the damper due to small amplitude motions about a steady state static off-center circular orbit. In this case, no cavitation is assumed, and the journal has no angular velocity, so direct stiffness cannot be calculated from the closed-form solution. Radial clearance, journal length, and journal eccentricity have a significant effect on fluid force and damping within a thin film damper. Fluid density does not affect fluid force or damping substantially, while fluid viscosity does. Both the closed-form solutions and computational fluid dynamics simulation compare well with each other and reflect these trends.

INTRODUCTION

The need for higher speed rotor operation has driven the need for efficient, robust, and reliable bearing dampers. Thin film dampers fulfill such requirements and greatly reduce vibration problems [1]. The thin-film damper generally surrounds the journal bearing. The outer housing of the journal bearing in contact with the thin-film is nonrotating. The movement of this housing can be approximated by either an elliptical orbit or circular orbit. This paper compares closed-form solutions of circular orbiting short-length bearings. A bearing is considered short when its length to diameter ratio is less than 0.5. Parametric studies during design can take a considerable amount of time when using 3D computational fluid dynamic (CFD) simulations. Starting with parametric studies using closed-form solutions (CFSs) streamlines the design process for building prototype damper systems. Once a range of damper geometric and fluidic parameters have been determined suitable for the needs of the bearing, 3D CFD simulations can be performed to finalize the design based on fluid and geometric characteristics determined from the CFSs.

CLOSED-FORM SOLUTIONS

Closed-form solutions for thin-film dampers have been developed for various configurations over the last century. Reynolds simplified the Navier-Stokes equations in an effort to develop an approximation for hydrodynamic lubrication in the 1800's [2]. Further simplifications to Reynold's equation approximation was made by assuming a short or long journal bearing, which was developed by Dubois and Ocvirk [3]. This paper uses the short bearing assumption for comparison to CFD calculations. The force response of the damper is obtained by integrating the pressure on the journal surface. Reinhart and Lund [4] further developed this approximation by solving for

force coefficients that include inertial effects for plain journal bearings by using the small perturbation technique. Vance [5,6] developed force coefficients under the assumption of small amplitude journal motion and that the reaction forces are proportional to journal displacements and velocity components through inertia and damping coefficients.

The following derivation of the force coefficients starts with the simplified Reynolds equation for hydrodynamic lubrication.

$$\frac{\partial}{\partial z}\left(\frac{h^3}{12\mu}\frac{\partial P}{\partial z}\right) = \frac{\partial h}{\partial t} + \frac{\omega}{2}\frac{\partial h}{\partial \Psi} \quad . \tag{1}$$

$$\Psi = \theta + \Phi \quad . \tag{2}$$

$$h = c + e\cos\theta \quad . \tag{3}$$

$$c = (D - D_j)/2 \quad . \tag{4}$$

Figure 1 illustrates the important parameters of the thin film damper. The short-length thin film damper model assumes that the damper is short in the z or axial dimension (L/D < 0.50); therefore, the pressure gradient in the circumferential or Θ direction is significantly smaller compared with the z-direction and can be ignored [7]. Thus, the flow is primarily in the axial direction.

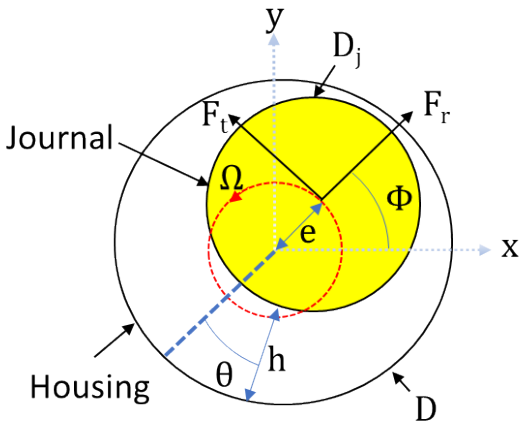

Figure 1: Squeeze film damper.

Where h is the film thickness at any location, e is the journal eccentricity, μ is the fluid viscosity, P is the pressure, z is the axial length of the journal, c is the radial clearance, and t is time. For this comparison, the journal rotation ω is assumed to be zero. Because stiffness terms are proportional to journal rotation, they too result in zero. Thus, Eq. 1 reduces to the following equation when journal rotation is zero:

$$\frac{\partial}{\partial z}\left(\frac{h^3}{12\mu}\frac{\partial P}{\partial z}\right) = \frac{\partial h}{\partial t} \quad . \tag{5}$$

The journal bearing eccentricity is fixed at some instantaneous static equilibrium. However, small amplitude motions from this equilibrium position are needed to determine damping and inertial characteristics [8]. When small amplitude motions or perturbations around the equilibrium occur, Δe and ΔΦ are incorporated into Eq. 5.

Eq. 5 is integrated twice with respect to z or the axial direction. The constants of integration are determined by applying the assumed open ends boundary condition at the top and bottom of the journal, P = 0 at z = ±L/2. $\varepsilon = e/c$ and $\dot{\varepsilon} = \Delta e/c$, which represent the eccentricity ratio and the change in eccentricity ratio, respectively are incorporated into the solution which becomes:

$$P = \frac{6\mu(\dot{\varepsilon}\cos\theta + \varepsilon\,\Delta\dot{\Phi}\sin\theta)}{c^2\,(1+\varepsilon\cos\theta)^3}\left(z^2 - \frac{L^2}{4}\right) \quad . \tag{6}$$

The forces acting on the bearing can be calculated by integrating the pressure over the journal surface, which is a function of both the journal axial length (z) from 0 to $L/2$ and the circumferential angle (θ) from 0 to α:

$$F_r = -\int_0^{\frac{L}{2}}\int_0^{\alpha} P\cos\theta\; D\; d\theta\; dz \quad . \tag{7}$$

$$F_t = -\int_0^{\frac{L}{2}}\int_0^{\alpha} P\sin\theta\; D\; d\theta\; dz \quad . \tag{8}$$

Note that D is the housing diameter. θ can be integrated between 0 and π assuming cavitation exists or between 0 and 2π assuming no cavitation. For the purposes of this study, no cavitation was assumed. The resulting equations from the double integration can be organized in terms of cross and direct damping and inertia force coefficients [5] for the short bearing assumption. The result of this integration produces only direct damping and inertia for coefficients:

$$F_r = -M_{rr}\ddot{\varepsilon} \quad . \tag{9}$$

$$F_t = -C_{tt}\varepsilon\,\Delta\dot{\Phi} \quad . \tag{10}$$

Where C_{tt} is direct damping coefficients, M_{rr} is the direct inertia force coefficients.

$$C_{tt} = \frac{\pi\mu D L^3}{2c^3(1-\varepsilon^2)^{3/2}} \quad . \tag{11}$$

$$M_{rr} = \frac{\pi\rho D}{12}\left(\frac{L}{c}^3\right)\left[1 - 2(1-\varepsilon^2)^{1/2}\right]\left\{\frac{(1-\varepsilon^2)^{1/2} - 1}{\varepsilon^2(1-\varepsilon^2)^{1/2}}\right\} \quad . \tag{12}$$

Note that $\varepsilon\Delta\dot{\Phi}$ and $\dot{\varepsilon}$ represent the tangential speed and normal acceleration of the orbiting journal. These equations were used to calculate the tangential and radial force components along with damping for various fluids, journal radii, clearances, and

orbit radii. These bearing characteristics were compared with a CFD code using the same geometric and fluidic parameters as described for the equations.

As mentioned earlier, these equations assume a short-length thin film damper with a length to diameter (L/D) ratio of <0.5. Several other limitations apply. Typically, thin films operate in low Reynolds number regimes; thus, these equations are limited to Reynolds number < 10 [9]. Finally, journal eccentricity (e) should be less than 75% of the radial clearance. In general, the thin film parameters used in this comparison were selected to remain within these constraints. The Reynolds number is calculated using Eq. 13.

$$Re = \frac{\rho c^2 \Omega}{\mu} \quad . \tag{13}$$

NUMERICAL ANALYSIS

ANSYS Fluent and ANSYS Mechanical were used to calculate the resulting forces on the journal based on a prescribed motion [10]. A model was created consisting of a cylindrical journal contained within a cylindrical casing for use in numerical analysis. Laminar transient conditions were assumed with no cavitation. Figure 2 shows an illustration of the model used in the analysis and the corresponding dimensions to the closed-form equations.

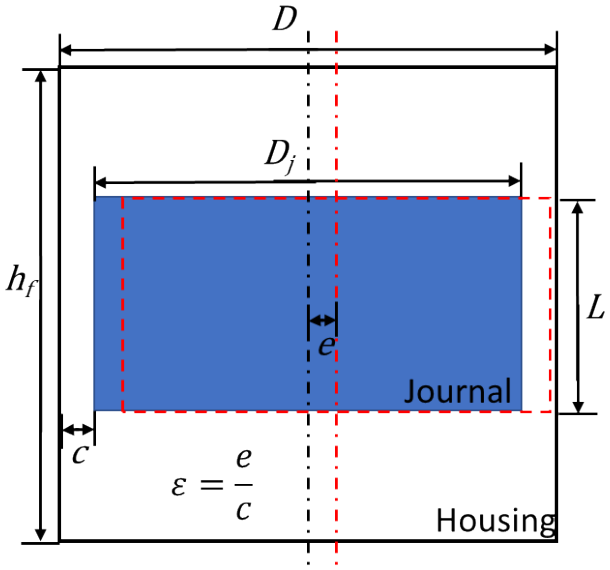

Figure 2: Analysis model parameters.

ANSYS Mechanical was used to prescribe the motion of the journal. The mechanical portion and fluid portion were coupled using the fluid-structure interaction capability in ANSYS Workbench. Mechanical supplied the displacement of the journal to Fluent, and Fluent sent the resulting fluid forces back to mechanical. This process was repeated for each time step in the analysis.

The model consisted of two separate meshes, one representing the journal and the second representing the fluid. Both the journal and fluid meshes are shown in Figure 3 and Figure 4, respectively.

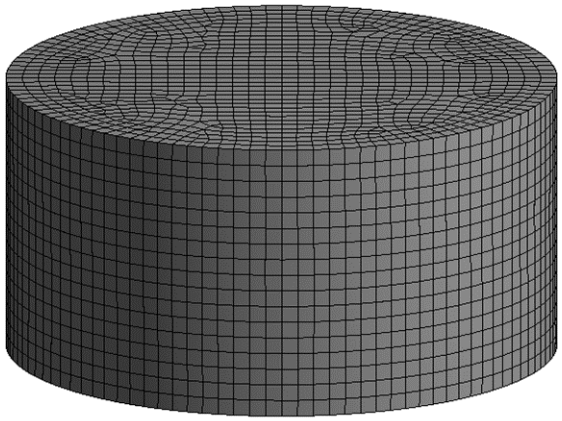

Figure 3: Journal mesh.

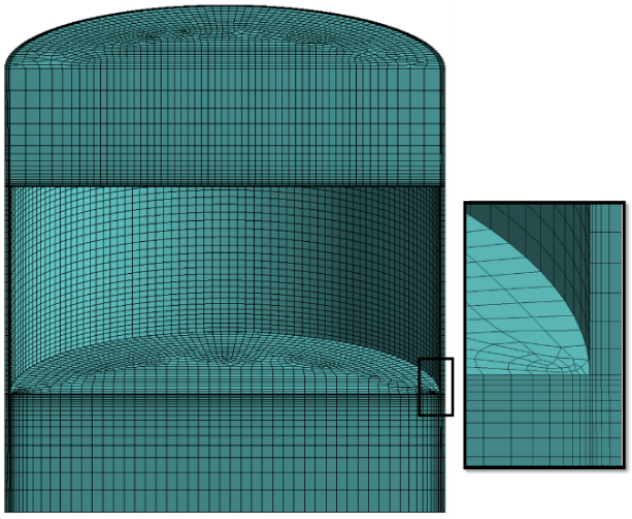

Figure 4: Fluid mesh.

Several fluid parameters, including density and viscosity, along with geometric parameters, such as journal height and orbit radius, were varied, and the resulting forces were computed using CFSs and ANSYS. Finally, the journal orbit frequency was varied, and forces and damping were computed using closed-form equations and ANSYS. Table 1 lists the fluid and geometric parameters used in the comparison. An orbital displacement was prescribed to the journal. The orbital motion was described by Eqs. 14 and 15. Figure 5 shows an example of the periodic applied displacements described by the two equations.

$$x\,disp = A\,sin(t\Omega) \quad . \tag{14}$$

$$y\ disp = A\ cos(t\Omega)\ . \quad (15)$$

A is the displacement amplitude, t is time, and Ω is the orbit frequency in rad/s. Note that at time zero, y displacement is equal to the maximum displacement amplitude; thus, the journal moves instantaneously to that location. This created unrealistic movement in the fluid, so the resulting fluid forces were ignored for several time steps from the beginning of the analysis. Fluid forces were recorded once the flow reached steady-state conditions.

Table 1: Thin film damper geometric (TFD) and fluid parameters compared

TFD Config.	μ Pa-s	ρ kg/m3	D m	Ω rad/s	L m	c m	e m	D_j m	ε e/c
1	0.1305	870	0.0512	1300	0.0254	0.0002	4.84E-05	0.0508	0.24
2	0.1305	870	0.0516	1300	0.0254	0.0004	4.84E-05	0.0508	0.12
3	0.1305	870	0.052	1300	0.0254	0.0006	4.84E-05	0.0508	0.08
4	0.1305	870	0.0525	1300	0.0254	0.00085	4.84E-05	0.0508	0.06
5	0.1305	870	0.053	1300	0.0254	0.0011	4.84E-05	0.0508	0.04
6	0.1305	870	0.056	1300	0.0254	0.0026	4.84E-05	0.0508	0.02
7	0.1305	870	0.052	1300	0.015	0.0006	4.84E-05	0.0508	0.08
8	0.1305	870	0.052	1300	0.02	0.0006	4.84E-05	0.0508	0.08
9	0.1305	870	0.052	1300	0.0225	0.0006	4.84E-05	0.0508	0.08
10	0.1305	870	0.052	1300	0.03	0.0006	4.84E-05	0.0508	0.08
11	0.1305	870	0.052	1300	0.035	0.0006	4.84E-05	0.0508	0.08
12	0.1305	870	0.052	1300	0.0254	0.0006	4.84E-06	0.0508	0.01
13	0.1305	870	0.052	1300	0.0254	0.0006	0.00025	0.0508	0.42
14	0.1305	870	0.052	1300	0.0254	0.0006	0.00035	0.0508	0.58
15	0.1305	1000	0.052	1300	0.0254	0.0006	4.84E-05	0.0508	0.08
16	0.1305	1450	0.052	1300	0.0254	0.0006	4.84E-05	0.0508	0.08
17	0.1305	1740	0.052	1300	0.0254	0.0006	4.84E-05	0.0508	0.08
18	0.06525	870	0.052	1300	0.0254	0.0006	4.84E-05	0.0508	0.08
19	0.19575	870	0.052	1300	0.0254	0.0006	4.84E-05	0.0508	0.08
20	0.261	870	0.052	1300	0.0254	0.0006	4.84E-05	0.0508	0.08
21	0.1305	870	0.052	1000	0.0254	0.0006	4.84E-05	0.0508	0.08
22	0.1305	870	0.052	1600	0.0254	0.0006	4.84E-05	0.0508	0.08
23	0.1305	870	0.052	2000	0.0254	0.0006	4.84E-05	0.0508	0.08

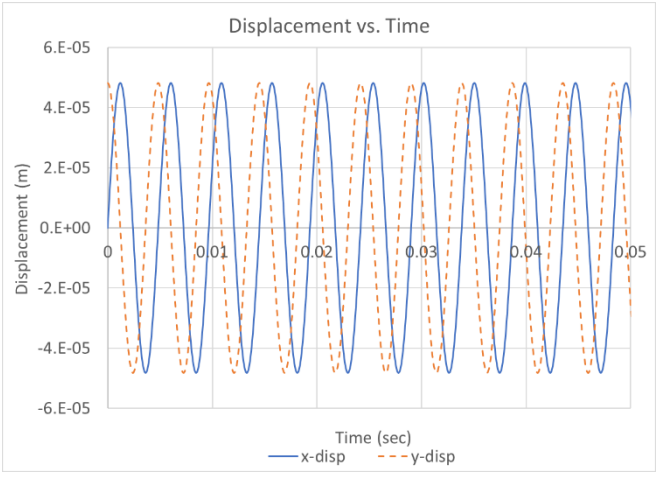

Figure 5: Journal enforced displacement.

The fluid portion of the analysis was set up to be laminar, with no slip side wall boundary conditions and pressure inlet and outlet boundaries at the top and bottom, respectively. The pressure was set to atmospheric at both pressure boundaries to simulate an open system per the requirement of the CFSs. Figure 6 shows a model schematic detailing the boundary conditions of the model.

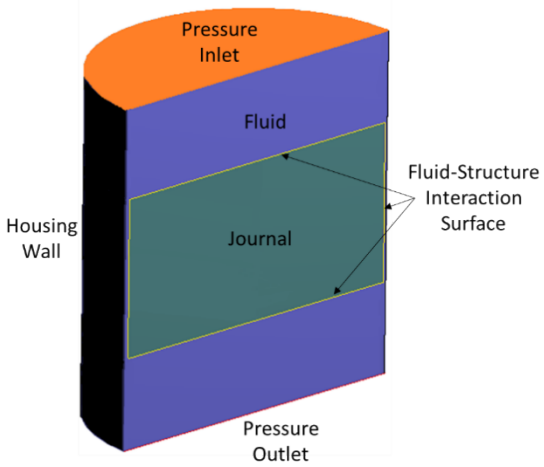

Figure 6: Analysis model boundary conditions.

The resulting *x* and *y* directional fluid forces acting on the journal were extracted over time. The total fluid force on the journal was calculated and compared with the computed force from the CFSs. Figure 7 shows an example of the resulting steady-state fluid forces for thin film damper configuration 3.

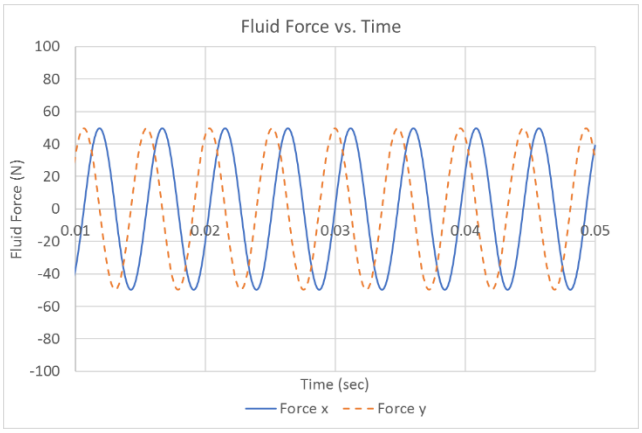

Figure 7: Steady-state fluid forces for thin film configuration 3.

The damping coefficient was calculated based on the phase angle between the applied displacement and the resulting fluid force. This was calculated plotting the normalized applied displacement in one direction and the normalized force in that same direction over time, as shown in Figure 8. The time span between the two curves was used to calculate the phase angle using Eq 16.

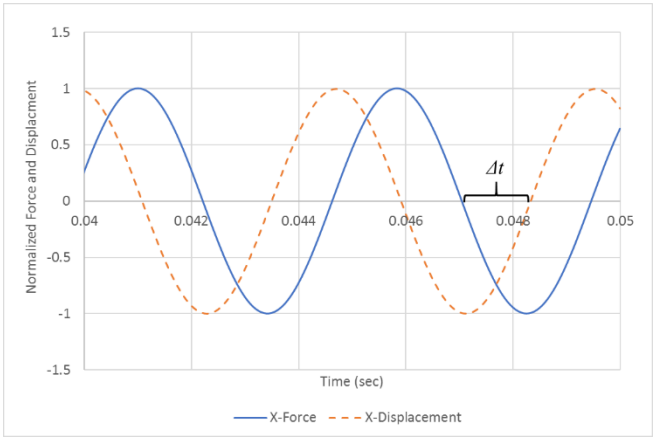

Figure 8: Normalized displacement and force versus time used to calculate phase angle.

$$phase\ angle\ (\emptyset) = \frac{\Delta t}{\left({}^{1}/_{\Omega}\right)} \quad . \tag{16}$$

Ω is the journal orbit velocity in rad/s, and Δt is the time difference between the displacement and force results where they cross the x axis. Once the phase angle for a thin film configuration was calculated, the damping coefficient was calculated using the following equation:

$$C_{CFD} = \frac{F \sin \emptyset}{\Omega X} \quad , \tag{17}$$

where F is the peak fluid force due to peak displacement X. The damping coefficient for the numerical analysis was compared with the CFS damping coefficient calculated by Eq. 11.

RESULTS AND DISCUSSION

Plots of the comparisons were made for each varied thin film parameter. Several parameters were selected so that the bounds of the CFSs were exceeded to observe how the comparison diverges. Some of the varied parameters produced very little to no changes in force and damping, as predicted by the CFSs. The numerical analysis predictions generally varied slightly for changes in these same parameters. Parameters that reduced the clearance between the journal and housing had the most drastic effect on the fluid force and damping. Both the CFSs and the numerical analysis show these effects. Figure 9, Figure 10, and Figure 11 show the fluid force and damping as a function of radial clearance, journal length, and journal eccentricity.

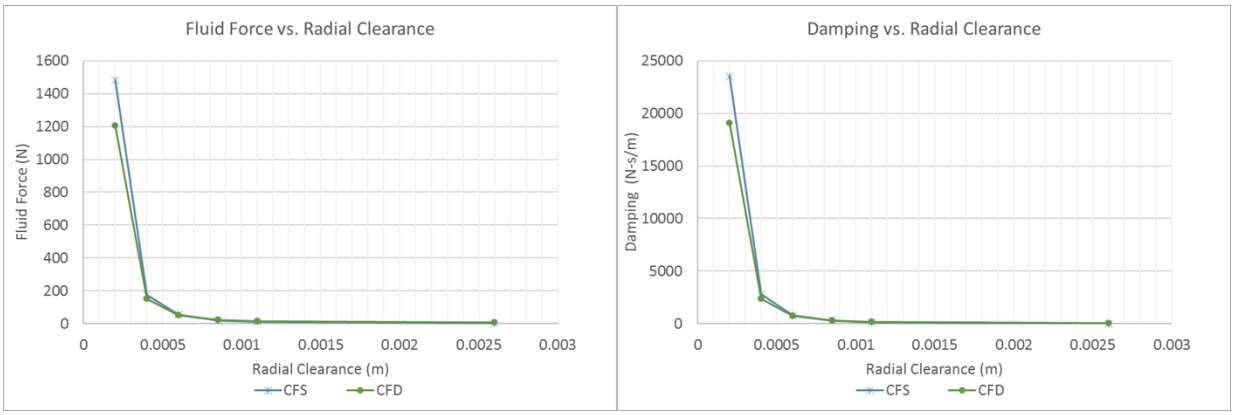

Figure 9: Fluid force and damping as a function of radial clearance.

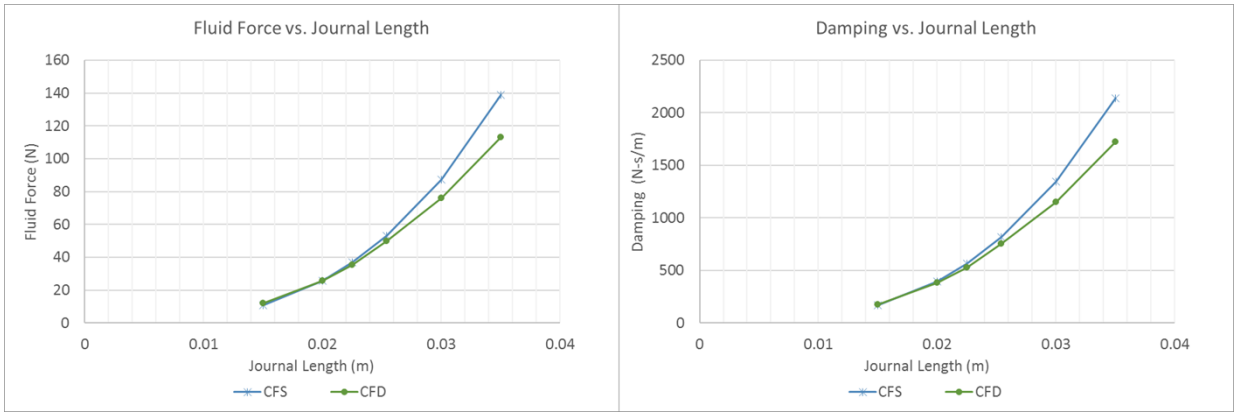

Figure 10: Fluid force and damping as a function of journal length.

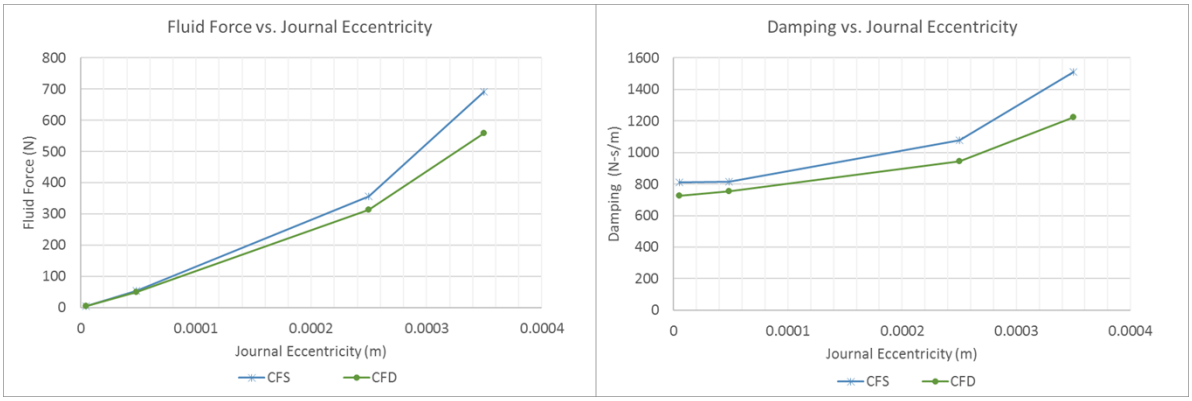

Figure 11: Fluid force and damping as a function of journal eccentricity.

Both the CFD and CFS results were close over the entire range of radial clearance considered. Both methods predicted a drastic increase in both force and damping when the radial clearance was reduced to 200 µm. Both the CFD and CFS both predicted an increase in force and damping with an increase in journal length. This is due to an increase in surface area in contact with the damping fluid. As the journal eccentricity increases both the fluid force and damping increase. This is result is consistent with the trend seen in reducing the radial clearance. As the eccentricity of the journal increases it distance to the wall decreases resulting in a higher force and damping.

Figure 12 shows the fluid force and damping as function of orbit velocity. The calculated damping from CFS has no dependency on orbit speed, however the force is proportional to orbit speed. The CFD calculation predicted a slight increase in damping with orbit speed. This is due to damping being calculated using the fluid generated force on the journal which is dependent on orbit speed as indicated in Figure 12. Both CFSs and CFD predict an increase in force as orbit speed increases.

The fluid force and damping were also calculated using the CFS based on various fluid densities and viscosities and compared with CFD as shown in Figure 13 and Figure 14 respectively. Fluid density did not have a significant influence on fluid force or damping. Fluid viscosity, however, had a substantial effect on both fluid force and damping. This is due to the increase in fluid shear force which is proportional to the fluid viscosity for Newtonian fluid. These trends are reflected in the comparison plots between the CFSs and the CFD model.

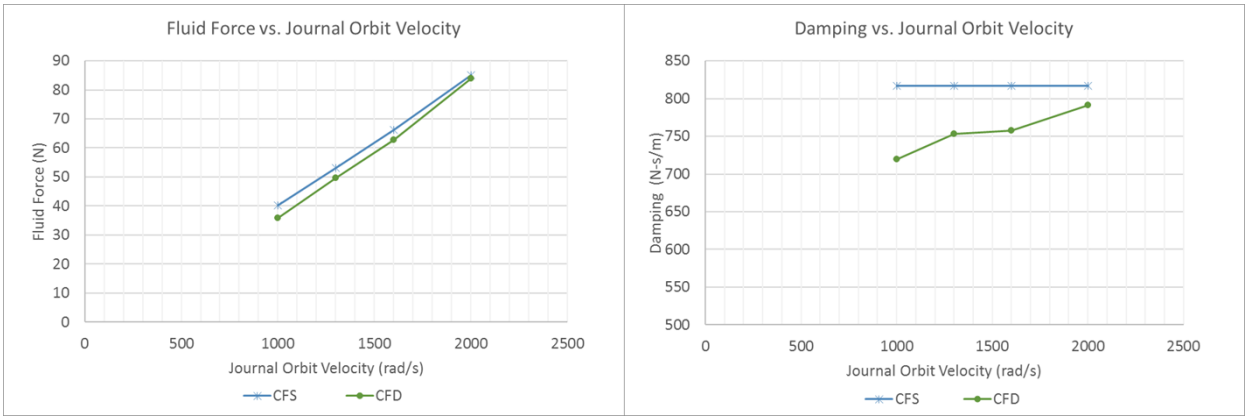

Figure 12: Fluid force and damping as a function of journal orbit velocity.

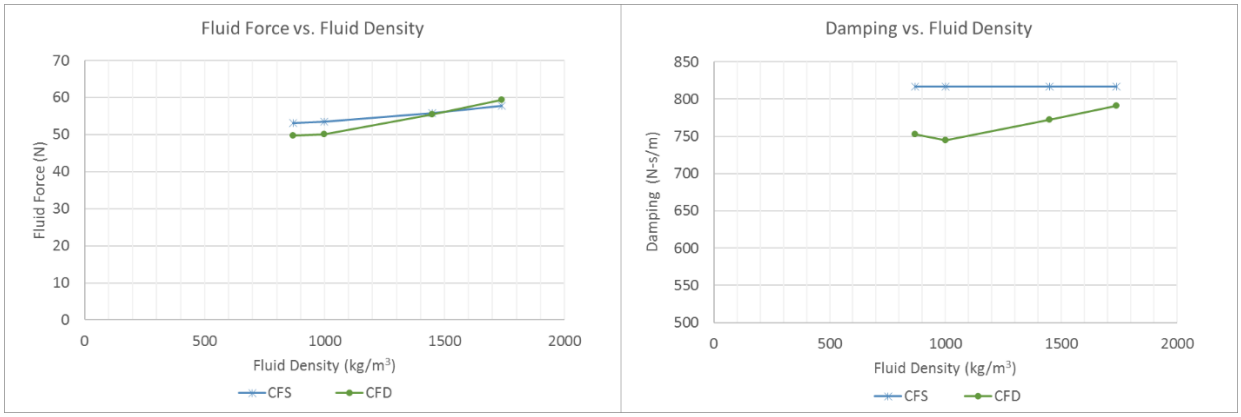

Figure 13: Fluid force and damping as a function of fluid density.

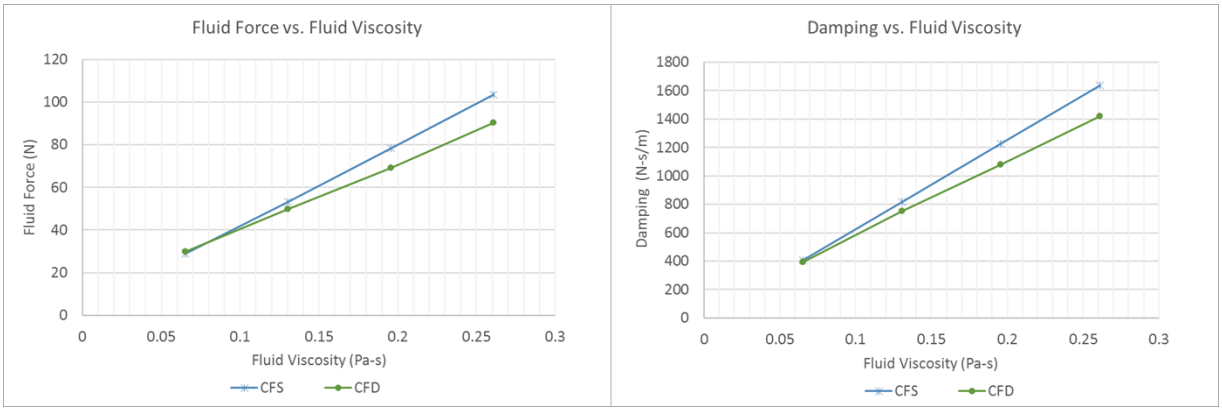

Figure 14: Fluid force and damping as a function of fluid viscosity.

CONCLUSION

The results of this study show good agreement between the CFSs and the CFD models. As mentioned previously, some geometric

and fluid properties were selected that exceeded the bounds of the CFSs. Many of the divergences between the CFSs and the CFD models as presented in the plots are a result of higher Reynolds numbers, which is in direct relation to fluid inertial effects. Also, the short thin film damper approximations used to derive the CFSs are not accurate at larger eccentricity and length to diameter ratios [11].

Generally, since the housing is non-rotating and its perturbations are small, cavitation should not occur. However, a more detailed analysis including cavitation should be conducted and compared with the closed form solutions if the rotor is expected to impart a significant amount of energy to the damper. Cavitation reduces the effectiveness of the damper and can negatively impact the entire rotor system. The ultimate objective in considering cavitation would be to eliminate it completely or significantly reduce it by design.

The CFSs are a good starting point in designing a thin film damper for rotor applications. The damper and fluid properties can be optimized to suit the needs of the system. Once these are determined by the CFSs, a more detailed numerical simulation can be performed to finalize the design. This design then can be used to develop a prototype for detailed testing.

NOMENCLATURE

A = displacement amplitude [m]
h = film thickness [m]
t = time [sec]
c = radial clearance [m]
C_{CFD} = damping from CFD
D = diameter of housing [m]
D_j = diameter of journal [m]
e = journal eccentricity [m]
Fr = radial force [N]
Ft = tangential force [N]
Fx = force in x-direction [N]
Fy = force in y-direction [N]
h_f = fluid height [m]
L = journal length [m]
P = pressure [Pa]
X = Peak Displacement [m]
z = journal axial length [m]
ε = eccentricity to radial clearance ratio
μ = fluid viscosity [Pa-s]
ρ = fluid density [kg/m^3]
Ω = journal orbit angular velocity [rad/s]
ϕ = Phase Angle [rad]

ACKNOWLEDGMENTS

This material is based upon work supported by the US Department of Energy, Office of Science.

REFERENCES

[1] H. R. Heidari and P. Safarpour. 2016. “Design and modeling of a novel active squeeze film damper.” *Mechanism and Machine Theory* 105: 235–243.

[2] Reynolds, O.: On the Theory of Lubrication and Its Application to Mr. Beauchamp Tower’s Experiments, Including an Experimental Determination of the Viscosity of Olive Oil. Phil. Trans. Roy. Soc. (London), ser. A, vol. 177, 1886, pp. 157-234.

[3] DuBois, G.B. and Ocvirk, F.W. 1955. Analysis derivation and experimental evaluation of short-bearing approximation for full journal bearings. National Advisory Committee for Aeronautics. Report 1157.

[4] Reinhardt, F. and Lund, J.W., 1975, “The Influence of Fluid Inertia on the Dynamic Properties of Journal Bearings, “ASME Journal of Lubrication Technology, 97(1), pp.154-167.

[5] J. M. Vance. 1988. *Rotordynamics of Turbomachinery*. vol. 9. Hoboken, NJ: John Wiley & Sons. ISBN 0471802581.

[6] L. San Andres and J. M. Vance. 1987. “Force Coefficients for Open Ends Squeeze Film Dampers Executing Small Amplitude Motions About an Off-Centered Equilibrium Position,” Tribology Transactions, 30(1), pp. 63-68.

[7] A. El-Shafei. 1988. “Dynamics of Rotors Incorporating Squeeze Film Dampers.” PhD Thesis, Massachusetts Institute of Technology, Boston, MA. https://dspace.mit.edu/bitstream/handle/1721.1/87804/20100750-MIT.pdf?sequence=2.

[8] C. Jia, H. Paug, W. ma, and M. Qiu, 2016 “Dynamic Stability Prediction of Spherical Spiral Groove Hybrid Gas Bearings Rotor System.” ASME Journal of Tribology, 139(2) 21701.

[9] L. D. Pietra and G. Adiletta. 2002. “The Squeeze Film Damper over Four Decades of Investigations. Part1: Characteristics and Operating Features.” *The Shock and Vibration Digest* 34(1): 3–26.

[10] ANSYS release 19.0 Mechanical and Fluent Workbench.

[11] S. Hamzhlouia, K. Behdinan, A Study of Lubricant Inertia Effects for Squeeze Film Dampers Incorporated into High-Speed Turbomachinery, Lubricants, 2017,5,43.